Journal of Applied Research and Technology

www.jart.icat.unam.mx

Journal of Applied Research and Technology 22 (2024) 125-137

Original

Identification of geothermal potential zone associated with land surface temperature derived from Landsat 8 data using split-window algorithm

Akhyar[a]* • C. A. Sary[b]

[a]*Department of Mechanical Engineering, Universitas Syiah Kuala, Jl. Syech Abdurrauf No. 7, Darussalam, Banda Aceh 23111, Indonesia*
[b]*Department of Geological Engineering, Faculty of Engineering, Universitas Syiah Kuala, Indonesia*

Received 10 16 2022; accepted 06 13 2023
Available 02 29 2024

Abstract: This study was conducted in the geothermal potential area of Mount Seulawah, Aceh province. The study was conducted using remote sensing methods to estimate and map the land surface temperature (LST). Data used in this study is Landsat 8 OLI and TIRS. Methods used in this study were split-window algorithm (SWA) to obtain the LST through NDVI analysis and landcover classification, and image enhancement to obtain the lineament density through visual interpretation referring to the results of band ratio and filter techniques. The results of the NDVI analysis show that the study area has a value in the range of -0.57 to 0.97. The results of the LST analysis show that the surface temperature in the area has a value in the range of 21.32 to 32.88 °C. Areas that have high LST values can be estimated as areas that have anomalies. Based on the results of the lineament density analysis, the higher density value in an area can indicate better permeability where geothermal manifestations come out. The direction of the lineaments that control the study area is dominated by the northwest-southeast following the direction of the main stress, namely the Seulimeum fault and the Aceh fault which also has a northwest-southeast direction. The overall results show that the Seulawah geothermal area has quite potential to be developed as a sustainable natural resource.

Keywords: geothermal, land surface temperature, Landsat 8, split-window algorithm, lineament density

*Corresponding author.
E-mail address: akhyar@usk.ac.id (Akhyar).
Peer Review under the responsibility of Universidad Nacional Autónoma de México.

1. Introduction

According to the Ministry of Energy and Mineral Resources, Indonesia has 40% of the world's geothermal reserves and only 8.9% has been explored and utilized (Ministry of Energy and Mineral Resources - Indonesia, 2022). Geothermal is spread throughout Indonesia, one of which is in the volcanic mountain in Aceh, namely Mount Seulawah. Information on the properties of the surface that has high potential value for exploration targets is represented in the form of hydrothermal alteration zones (Bedini et al., 2007; Nouri et al., 2012; Pour & Hashim, 2012; Rani et al., 2020). Monitoring of hydrothermal alteration has the advantage of conserving geothermal systems that are of cultural significance or economically important (Bromley et al., 2010). In a hydrothermal investigation, remote sensing has a key role in the part of "identification" through its sensor's ability to locate the surface expression of a geothermal feature by surface object temperature (Heasler et al., 2009).

Remote sensing techniques have been used for mineral exploration and are helpful in mapping the altered minerals (Rani et al., 2020). Numerous remote sensing sensors have been utilized for alteration mapping through visual and automated interpretation. Waldhoff et al. (2008) successfully mapped a wide range of minerals for alteration zones utilizing Multispectral and Hyperspectral images. Multispectral images including Landsat-8 OLI and Landsat 7 ETM+ are mostly used for hydrothermal alteration zone mapping (Amara et al., 2019; Osinowo et al., 2021; Southworth, 2004). The spectral characteristics contained in Landsat data through its pixel value are valuable for hydrothermal alteration zone recognition (Masoumi et al., 2016). Şener & Şener (2021) used Landsat 8 OLI TIRS in determining the geothermal potential involving several parameters including land surface temperature (LST), geological formations and lineaments, and hot springs.

LST is the Earth's surface temperature where the heat and radiation from the sun are reflected, absorbed, and refracted (Mishra et al., 2020). LST is a key parameter for volcano thermal activity monitoring, and it typically can be estimated from thermal infrared data of Landsat data products (Mia et al., 2019). The recent products of Landsat data have been used including Landsat 5, 7, and 8 for LST extraction with other driven parameters through different retrieval algorithms and provided good accuracies (Sekertekin & Bonafoni, 2020). To perform the LST retrieval from Landsat data, thermal channels are required, and in this case, Landsat 8 OLI/TIRS is the only Landsat product that has two thermal channels, 10 and 11 (Alipour et al., 2003). A method for retrieval of LST from the two thermal channels of Landsat 8 can be performed through the Split-window algorithm (SWA).

SWA was developed by Rozenstein et al. (2014) leading to progress in the determination of LST on Landsat-8 TIRS. SWA is the most widely used algorithm for LST extraction through surface emissivity information from TIRS data and it highly influences the sensitivity of the algorithm (Zhang et al., 2019). SWA was proven to generate good stability through analysis of the sensitivity of Landsat-8 TIRS (Jin et al., 2015). SWA normalizes the value of surface temperature at bands 10 and 11 so that obtains the best value representing field condition. SWA method corrects the atmospheric effects based on differential absorption in the adjacent infrared bands (Tan et al., 2016). Besides emissivity information, SWA requires other input parameters including the land cover of the interest area to know the temperature of each land cover class (Twumasi et al., 2021). Land cover mapping is useful for numerous environmental monitoring and resources management applications including hydrothermal potential mapping (Shi & Yang, 2015).

The LST retrieval for hydrothermal alteration zone mapping is inseparable from geological structural elements (Twumasi et al., 2021). The geological structure is the main factor that controls the distribution of geothermal manifestation. An area with high fault and fracture density has a high probability of the distribution of geothermal manifestation and it can be utilized for mapping hydrothermal alteration (Sheikhrahimi et al., 2019).

This study focuses on using Landsat-9 imagery to estimate and map the hydrothermal alteration through information extraction of LST using the Split-window algorithm and ancillary data such as NDVI and lineament. The benefit of this study is to be a reference in further scientific research using Landsat 8 image, to identify the high hydrothermal potential zone for environmentally friendly geothermal exploration management.

2. Materials and methods

2.1. Study area

Aceh is one of 34 Indonesian provinces located on the western end of the Sumatran archipelago. As a region at the western end of Indonesia, the map of Aceh has a geographical position between 2°-6° north latitude and 95°-98° south latitude with an altitude of 125 meters above sea level (Fadhil & Akhyar, 2023; Farhan & Akhyar, 2017; Sugianto et al, 2023). Mount Seulawah was formed because of the Indo-Australian plate moving relative to the north subduction under the Eurasian continental crust plate. As a result of the subduction, there was a process of melting of the Indo-Australian oceanic crust into magma which then broke through to the surface through the weak zone and then formed Mount Seulawah. The

manifestation of Mount Seulawah is in the form of hot springs, namely Ie Seu Um and Ie Ju, and there are also manifestations in the form of mud pools, altered rocks, fumaroles, and steamy ground. Figure 1 presents the study area map, the region to be analyzed (the study area) is about 86.14 km^2.

The study region was chosen because Mount Seulawah Agam and its surroundings had surface geothermal manifestations. The Ie-Seu'um, Ie-Brôuk, Ie-Jue, and Van-Heutz crater hot springs and hot steam in this region are geothermal manifestations (Idroes et al., 2019). The faults and fractures that are created by the tectonic activity in the earth's crust have the potential to serve as channels for geothermal fluids to flow toward the surface (Hermawan & Rezky, 2011).

2.2. Materials

This study uses Landsat-8 data with a sensing date of December 04, 2021. Some information can be extracted from its bands (OLI and TIRS) including NDVI, LST, and lineament. The image was selected considering the less cloud cover in the study area to get the real LST values only from the land surface without being interfered with by cloud values. Data was downloaded from the United States Geological Survey (USGS) at https://glovis.usgs.gov/ and data has been calibrated radiometrically and geometrically.

Applications for remote sensing and analysis of Landsat-8 imagery have been used. This application can identify geothermal potential zones related to ground surface temperature through a split-window algorithm. The following remote sensing applications require the following system configurations: operating systems include Windows, Linux, and Windows; 4 GB or more of disk space for installation; Memory (RAM): 8GB minimum; a graphics card with at least 1 GB of Memory and support for OpenGL 2.0 or later, a minimum of 2 computing cores, and a recommendation of 4 or more (Farhan, 2024).

An essential step in processing remote sensing data from satellites such as Landsat 8 is radiometric and geometrical calibration. The process of radiometric calibration involves converting the digital numbers (DN) that the satellite acquired into physical units of radiance or reflectance. Digital number (DN) typically assigns a value to a pixel in the form of a binary integer in the range of 0 to 255 that represents the strength of the land cover reflectance. First, the Landsat 8's unitless DN was converted to top-of-atmosphere (ToA) radiances across all bands (LToA). A correction for atmospheric influences was necessary because surface leaving radiance from satellite pictures was altered by the atmosphere. As the whole research area overlapped inside a single image and there was no cloud cover effect, the atmospheric correction could be managed using a straightforward model method (Li et al., 2014).

The processing of remote sensing data from satellites Landsat 8 also includes geometric calibration, which is a crucial phase. The function of image-to-map rectification is that the map being used should have more precise coordinates and a projection system so that it may be utilized as a reference by the image. This kind of geometric adjustment is always necessary for remote sensing applications that call for precise measurements of distance, direction, and area. Choosing a pair of coordinate coordinates on the image (row-column) and the map (x-y/ latitude-longitude), eliminates geometric distortion in the image. We will determine the coefficients of the transformation equation that transforms the image coordinate system into the map coordinate system (Budi & Akhyar, 2022).

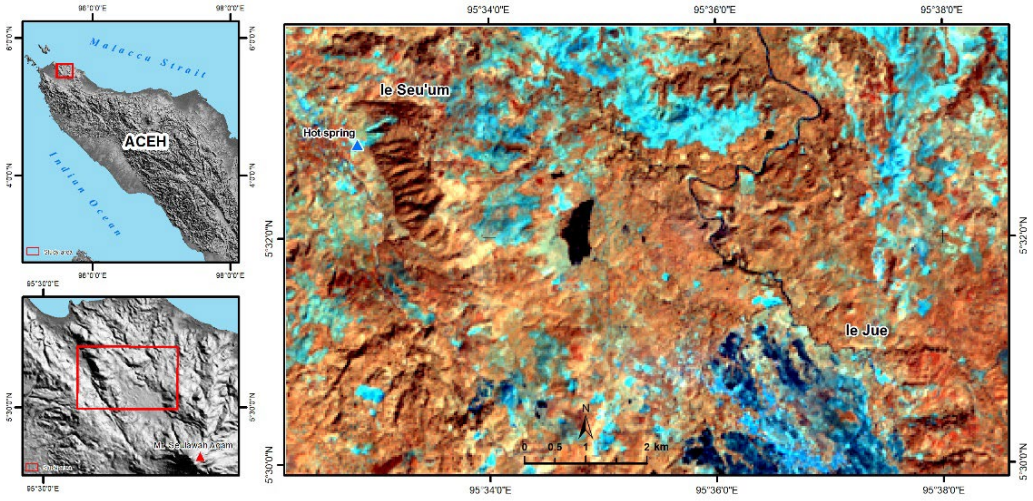

Figure 1. Study area.

2.3. Methods

In this study, to estimate the hydrothermal potential, the hydrothermal alteration was identified through some processing steps; land surface temperature (LST) retrieval consisted of NDVI calculation and land cover classification, lineament extraction consisted of spectral and spatial enhancement, and potential hydrothermal distribution mapping, flow chart as shown in Figure 2.

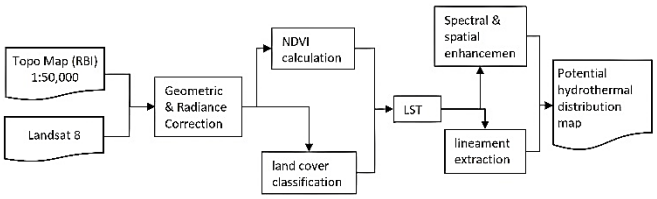

Figure 2. Study flow chart.

Split-window algorithm, SWA uses some variables from 10 and 11 bands, including 1) brightness temperature, mean, and difference in land surface emissivity (Saleh, 2017). 2) emissivity and algorithm transmittance (Li & Jiang, 2018; Rozenstein et al., 2014). SWA works by taking separately into account atmospheric water vapor, surface emittance, and air surface temperature difference and results from the land surface temperature utilizing a formalism valid for a wide range of atmospheric water vapor and surface emittance (Ulivieri et al., 1994). Each object on the earth's surface has a different emissivity through its radiance transmission (Sutanto, 1987). The emission of energy from the Earth's surface in bands 10 and 11 is functioned to convert land cover type into emissivity value units (Southworth, 2004). Atmospheric transmission is obtained from the conversion of water vapor using only reflectance value from MODIS (Rozenstein et al., 2014).

Lineament extraction, in this study, applied two image enhancement techniques: spectral enhancement and spatial enhancement. The main purpose of image enhancement is to process the image so that the result is more compatible than the original image for a specific application, by enhancing the contrast and removing the noises to increase the image quality (Saleem & Razak, 2014). The change of image resulting from the band ratios technique was the enhancement of spectral variations of target anomalies (lineaments) as seen in Figure 3. It refers to Sadiya et al. (2016) that found a correlation between locations with purple hues and locations with the prevalence of lineaments. The band ratios technique was performed in this study to enhance the appearance of geological units by discriminating anomalous pixels to generate the alteration map using spectral bands, which is based on the multiplication, division, addition, and subtraction of distinctive bands (Askari et al., 2018; Maleki et al., 2021).

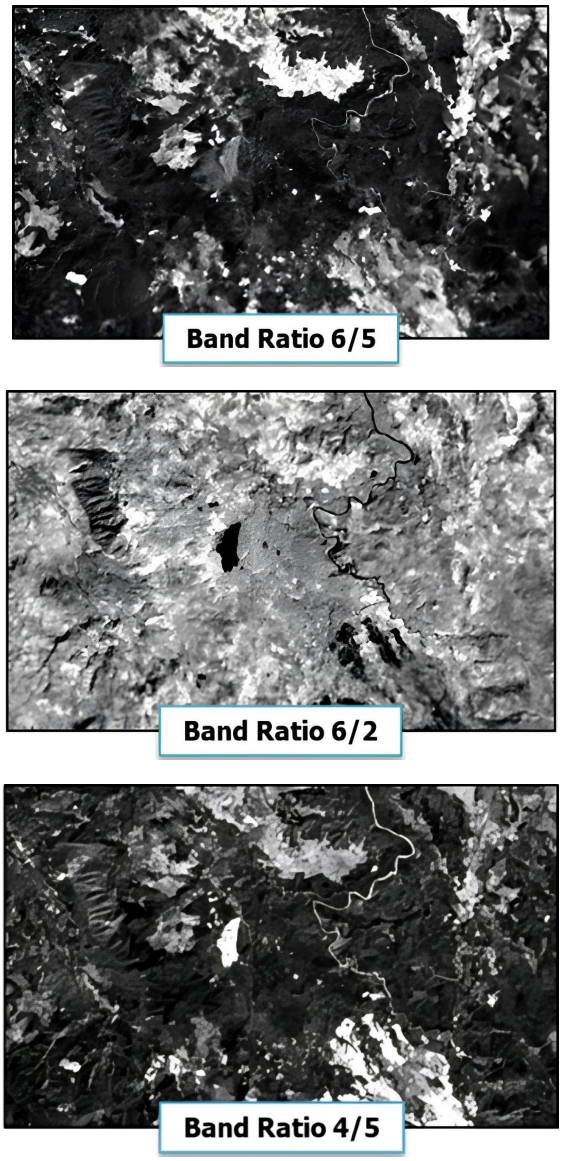

Figure 3. Band ratio-based images.

The result of spectral enhancement was forwarded to the spatial enhancement process examining filter technique on different image samples including band ratio 6/2, composite 567, and band ratio 6/2, 6/5, 4/5, as seen in Figure 4. High pass filtering was chosen in this study as a fundamental operation for sharpening the image display bypassing the high frequencies and attenuating frequencies lower than the cut-off frequency (Makandar & Halalli, 2015). Due to the small study area, lineament extraction was performed by visual/manual interpretation that enabled the interpreter to export lines accurately. Interpretation of lineament relies on the use of brightness information and the identification of features in the image.

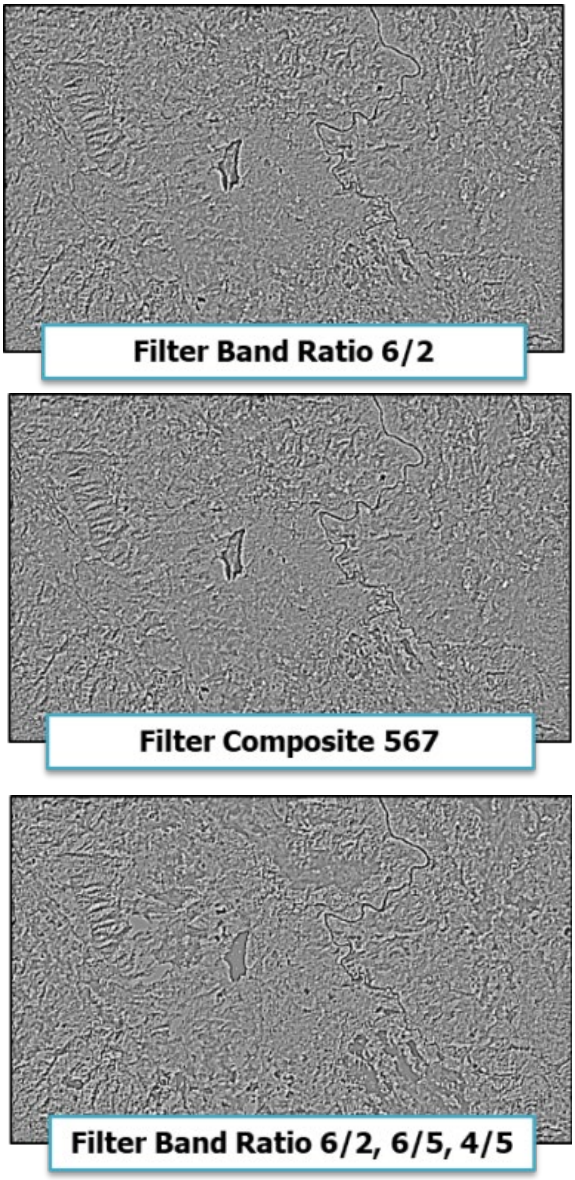

Figure 4. High pass filtering-based images.

The process of constructing the geothermal potential map can be done through spatial analysis by involving the integration of several parameters such as LST and lineament density (Omwenga, 2020). Geographic information systems (GIS) can be utilized as a decision-making tool to target the geothermal zone potential indicating the high-temperature geothermal resources (Dezayes et al., 2022). This integration can estimate the areas with high potential for the geothermal field through weighted overlay analyses (Rahmati et al., 2019). This technique overlays several parameters in the form of a raster and uses the common measurement scale and weights of each parameter according to its importance. This study determined the impact factors of parameters in weighted overlay referring to weighted information models by Zhao et al. (2021) which found the LST value as the highest impact factor in geothermal potential estimation.

3. Results and discussion

3.1. NDVI analysis

The range of NDVI values in the Ie Seu Um and Ie Ju areas is in the range of -0.573092 to 0.979054. The rare vegetation class has a value of -0.573092 to 0.1 represented by a white–green color. This area is interpreted as an area with grass and shrubs. While the dense vegetation class range is from 0.7 to 0.9 represented by a dark-green color. Thus, this area is interpreted as a dense forest area. Geothermal manifestation areas of Um and Ie Ju seen in Figure 5 are classified as dark green but in the field, the area is an empty land due to the manifestation, however, because the area is small so through remote sensing it is still interpreted as part of a dense forest.

The surface temperature of an area is very dependent on its vegetation density. The above Figure 5 shows the distributions of high and low vegetation density. Good vegetation shows low surface temperature values. Meanwhile, areas of poor vegetation have high surface temperature values.

3.2. Land cover classification

Figure 5 shows the land cover map of the study area. The classification was conducted referring to the threshold value of the NDVI map. The study area contains five classes, namely dry bare land which is marked in red, vegetation with high density, which is marked in green, vegetation with low vegetation density which is marked in light green, and water body which is marked in blue, and wet bare land which is marked in brown. The geothermal manifestation area, namely the Ie Seu Um and Ie Ju areas based on remote sensing, is a green area or an area with low density, while based on field data, the two areas are included in an empty area due to the high temperature that appears on the surface in the form of the eye hot springs, steamy ground, mud pool, and altered rock (Figure 6).

3.3. Land surface temperature analysis

Based on Landsat 8 image processing as seen in Figure 7, it can show that the surface temperature in the study area around Mount Seulawah has a range value of 21.32 to 32.88 °C. The distribution of low LST that has a temperature of 21.32 °C which is indicated by green to ancient colors on the map is more dominant than areas with high LST. This is the influence of high-density vegetation in the form of forests. The distribution of high LST which has a temperature of around 32.88 °C is shown in red on the map (Figure 7). Ie Seu Um and Ie Ju hot springs are two of Mount Seulawah's manifestations. Mud pools, altered rocks, fumaroles, and steamy ground are

also manifestations in the form. Field checking at Seu Um and Ie Ju is shown in Table 1, together with specific temperature measurement data.

As seen in the hot spring manifestation areas validated in the field by measuring the temperature (Figure 7), Ie Ju and Ie Seu Um hot springs have high LST. High LST is influenced by the presence of geothermal manifestations below the surface which affects the surface temperature. Geothermal manifestations can be used as a review of the geothermal potential on Mount Seulawah.

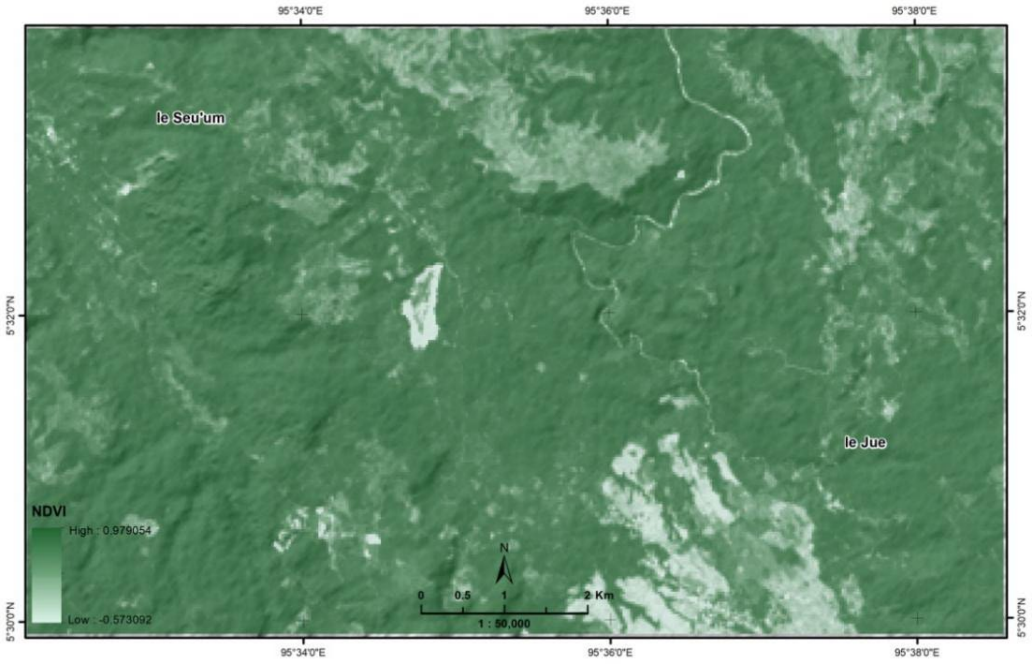

Figure 5. NDVI map of the study area.

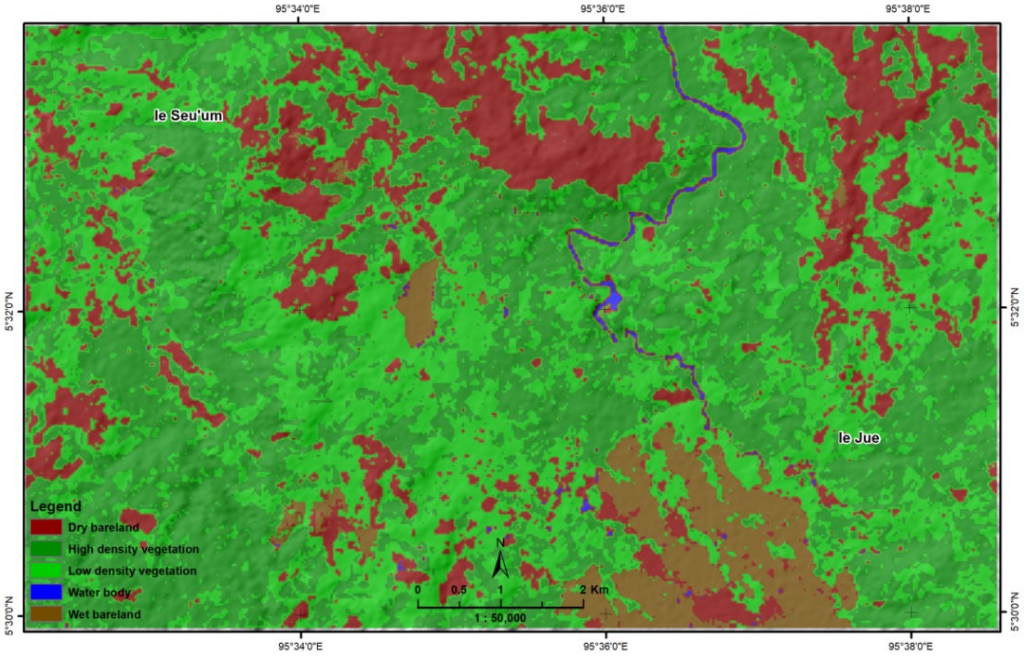

Figure 6. Land cover map of the study area.

3.4. Lineament density analysis

Figure 8 shows the lineament density map generated from the visual interpretation of lineament. The lineament density map is used to interpret the permeability in several study areas. The higher density value can indicate that the area has better permeability than the area with a lower density. Based on Figure 8, it can be interpreted that several areas have a higher density value as seen in the red image. Areas that have good permeability are places where geothermal manifestations come out (weak zones).

Interpretation in Figure 8 shows that weak zones can be formed due to several things, namely due to the presence of primary and secondary geological structures. The direction of the lineaments in the study area is northwest-southeast. This direction follows the direction of the main stress, namely the Seulimeum fault and the Aceh fault which also has a northwest-southeast direction.

3.5. Geothermal potential mapping

Based on the results of the LST map and lineament density map, a map of geothermal potential is obtained. In Figure 9, there are 3 color groupings, namely areas with red color which have high geothermal potential, while those colored orange have moderate geothermal potential, while areas with yellow color indicate areas that have low geothermal potential.

Based on the map result in Figure 9, the Seulawah geothermal potential area based on the map is in the eastern area of Ie Seu Um because the area has a high surface temperature, there is an important level of lineament density, and the vegetation in this area varies from water bodies to moderate. This area also has 5 main components of the geothermal system, which have geothermal manifestations in the form of Ie Seu Um and Ie Ju in the form of hot springs, steamy ground, alteration rock, and mud pools. In addition, it has a reservoir which is marked by the Ie Seu Um spring which has a high chloride element which is interpreted as the Ie Seu Um spring is close to the reservoir. It has covered rocks in the form of andesite to dacite volcanic rocks which have poor permeability. It has a structure that serves as a path for geothermal fluids to outflow and inflow. This structure can be seen in the geothermal prospect area with high lineament density values. The main component of a geothermal system is the presence of a heat source.

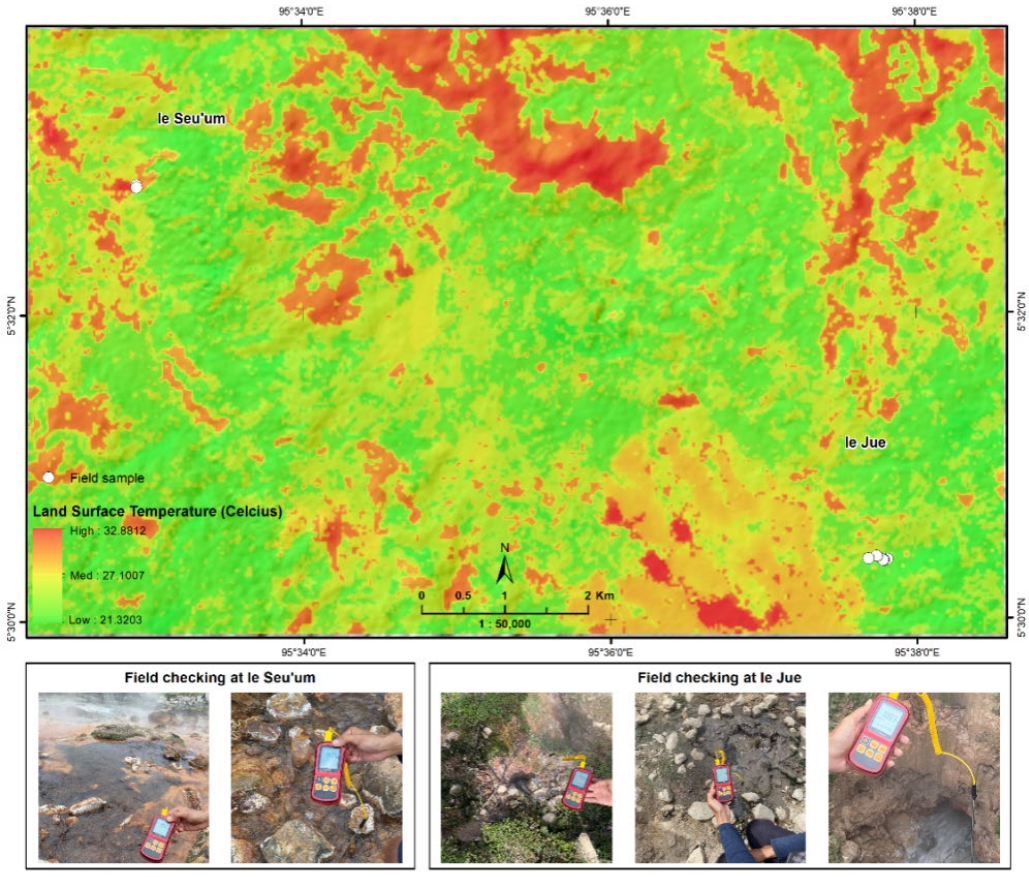

Figure 7. Land surface temperature map of the study area.

Table 1. Detailed temperature measurement data, at the field checking Seu Um and Ie Ju.

Locations	No.	Tempe-rature (°C)	Average temperature (°C)	Coordinate		Elevation (masl)	Manifestation type
				N	E		
Ie Seu Um	Point 1	88.1	88.4	5° 32'51"	95°32'55"	70	Hot springs
		88.6					
		88.5					
	Point 2	89.2	89.2	5° 32'50"	95°32'55"	70	Hot springs
	Point 3	89.2	88.7	5° 32'50"	95°32'55"	70	Hot springs
		87.7					
		89.1					
Ie Ju 1	Point 1	100.3	100.1	5° 30'23,23"	95°37'47,36"	265	Hot mud
		99.8					
		100.2					
	Point 2	76.4	78.5	5° 30'22,82"	95°37'47,14"	260	Steam ground and pits
		76.5					
		82.5					
	Point 3	103.7	104.1	5° 30'23,24"	95°37'48,44"	260	Steamy ground and altered rock
		105.1					
		103.6					
	Point 4	101.1	101.7	5° 30'22,90"	95°37'47,03"	265	Steamy ground
		101.9					
		102.1					
Ie Ju 2	Point 1	101.2	101.9	5° 30'22,87"	95°37'46,64"	250	Hot mud
		101.5					
		102.9					
	Point 2	104.4	103.8	5° 30'22,87"	95°37'46,64	250	Hot mud
		102.5					
		104.5					
	Point 3	105.2	105.0	5° 30'24,38"	95°37'44,41	250	Hot mud
		105					
		104.8					
	Point 4	105.9	105.5	5° 30'24,56"	95°37'44,10"	250	Hot mud
		106					
		104.5					
Ie Ju 3	Point 1	105.2	104.9	5° 30'23,72	95°37'40,95"	240	Hot springs
		107.6					
		102					
	Point 2	107.9	105.6	5° 30'23,55"	95°37'40,84"	240	Hot springs
		104.2					
		104.6					

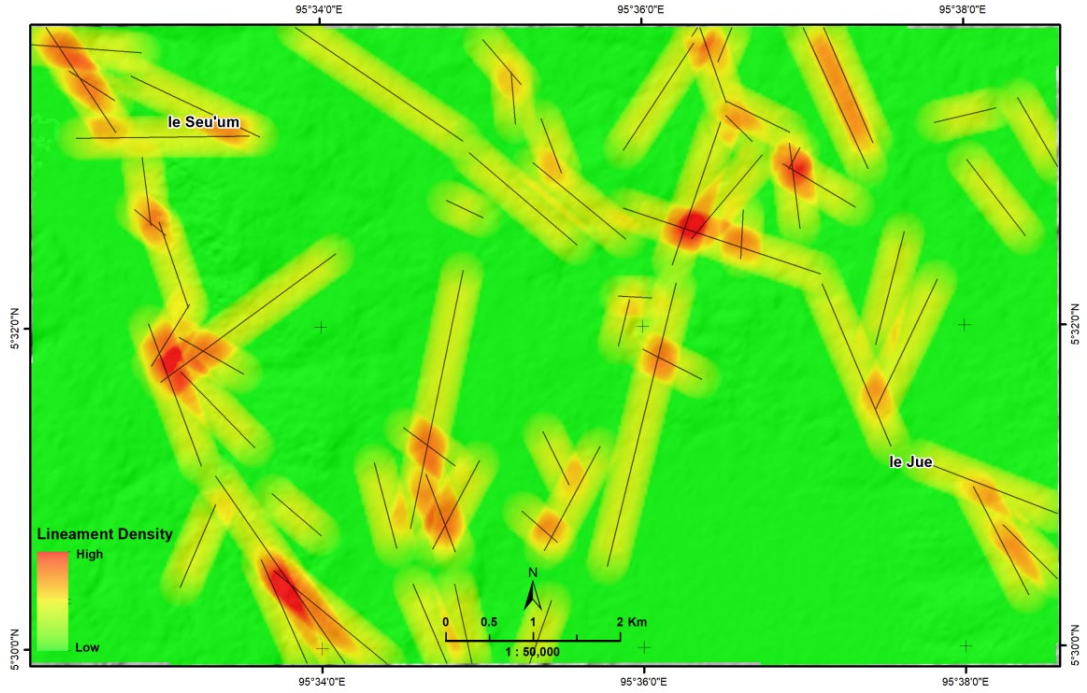

Figure 8. Lineament density map of the study area.

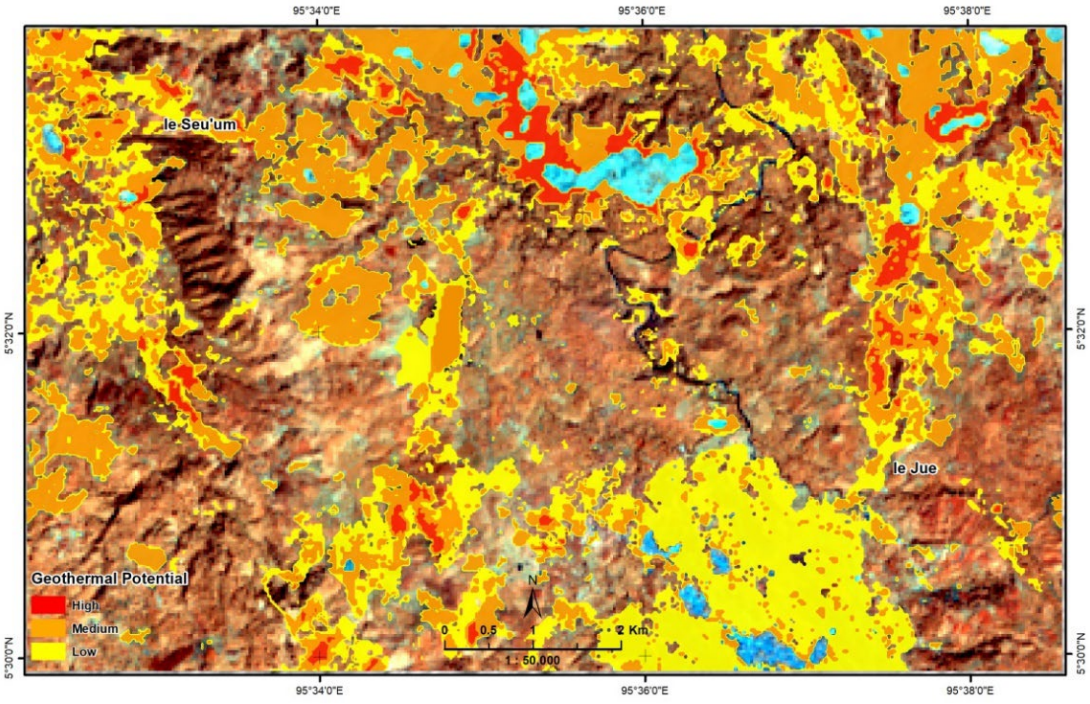

Figure 9. Geothermal potential map of the study area.

4. Conclusions

This study tries to identify the geothermal potential of Mount Seulawah, Aceh. The study was conducted based on a surface temperature map using remote sensing methods. It is also based on NDVI maps and lineament density. The results of the NDVI map show that the Mount Seulawah area is dominated by dense vegetation. In the Ie Seu Um and Ie Ju geothermal manifestation areas shown in the picture they are classified as dense vegetation but, in the field, the area is an empty land due to the manifestation, but because the area is small through remote sensing it can still be interpreted as part of a dense forest. The vegetation density map is also related to the surface temperature. Good vegetation exhibits low surface temperatures. While the area of poor vegetation has a high surface temperature value.

Based on the distribution map of the soil surface temperature, the geothermal manifestation areas of Ie Ju and Ie Seu Um have high LST. High LST is influenced by geothermal manifestations below the surface which affect the surface temperature. Geothermal manifestations can be used as geothermal potential on Mount Seulawah. The LST results were also validated by measuring the temperature in the field. Meanwhile, the results of the straightness density map show that the ie sum and ie ju manifestation areas have good density values because they are in the weak zone. Weak zones can be formed due to several things, namely due to the presence of primary and secondary geological structures. The direction of the lineaments in the study area is northwest–southeast. This direction follows the direction of the main stress, namely the Seulimeum fault and the Aceh fault which also has a northwest-southeast direction.

According to the interpretation of the NDVI, LST, and lineament density maps, the geothermal prospect area is in the eastern area of the Ie Seu Um manifestation. The soil surface temperature in this area is at a moderate to an elevated level and a vegetation density level from medium to low and there are many structures as outflow and inflow pathways.

Conflict of interest

The authors have no conflict of interest to declare.

Acknowledgements

We would like to thank Mr. Muhammad Budi for his support during this analysis.

Funding

The authors received no specific funding for this work.

References

Alipour, T., Sarajian, M.R., & Esmaeily, A. (2003). Land Surface Temperature Estimation from Thermal Band of Landsat Sensor, Case Study: Alashtar City. *The International Archives of the Photogrammetry, Remote Sensing and Spatial Information Sciences, XXXVIII-4/C7.*

Amara, B.N., Aissa, D.E., Maouche, S., Braham, M., Machane, D., & Guessoum, N. (2019). Hydrothermal alteration mapping and structural features in the Guelma basin (Northeastern Algeria): contribution of Landsat-8 data. *Arabian Journal of Geosciences, 12(94).*
https://doi.org/10.1007/s12517-019-4224-4

Askari, G., Pour, A. B., Pradhan, B., Sarfi, M., & Nazemnejad, F. (2018). Band ratios matrix transformation (BRMT): a sedimentary lithology mapping approach using ASTER satellite sensor. *Sensors*, *18*(10), 3213.
https://doi.org/10.3390/s18103213

Bedini, E., van der Meer, F., & van Ruitenbeek, F. (2007). Use of HyMap imaging spectrometer data to map mineralogy in the Rodalquilar caldera, southeast Spain. *International Journal of Remote Sensing, 30(2)*, 327–348.
https://doi.org/10.1080/01431160802282854

Bromley, C., van Manen, S. M., & Graham, D. (2010). Monitoring surface geothermal features using time series of aerial and ground-based photographs. In *AGU Fall Meeting Abstracts* (Vol. 2010, pp. IN33B-1308).

Budi, M., & Akhyar (2021). Green open space detection and mapping using planetscope-3a image with vegetation index approach and supervised classification in Banda Aceh, Indonesia. In *Forum Geografic* (Vol. 20, No. 2).
https://doi.org/10.5775/fg.2021.034.d

Dezayes, C., Famin, V., Tourlière, B., Baltassat, J., Bénard, B. (2022). Potential areas of interest for the development of geothermal energy in La Réunion Island based on GIS analysis. *Journal of Volcanology and Geothermal Research*, 421, 1-13,
https://doi.org/10.1016/j.jvolgeores.2021.107450

Fadhil A. M., & Akhyar (2023). Visual and semi-automated interpretation methods for urban flood detection using SAR Sentinel-1A image: study case in North Aceh Regency, Indonesia. *Disaster Advances Vol. 16 (2) February (2023), Disaster Advances; Vol. 16(2),* 30-40.
https://doi.org/10.25303/1602da030040

Farhan, A., & Akhyar, H. (2017). Analysis of tsunami disaster map by geographic information system (GIS): Aceh Singkil-Indonesia. In *IOP conference series: earth and environmental science* (Vol. 56, No. 1, p. 012002). IOP Publishing. https://doi.org/10.1088/1755-1315/56/1/012002

Farhan, A., Nasution, A.I. & Akhyar (2024). Earthquake disaster map using GIS analysis: a case study of Bener Meriah-Aceh, Indonesia. Arabian Journal of Geosciences, 17(53), https://doi.org/10.1007/s12517-023-11850-y

Heasler, H.P., Jaworowski, C., & Foley, D. (2009). Geothermal systems and monitoring hydrothermal features. *Geological Monitoring: Boulder, Colorado, Geological Society of America*, 105–140. https://doi.org/10.1130/2009.monitoring(05)

Hermawan, D., & Rezky, Y. (2011). Delineasi daerah prospek panas bumi berdasarkan analisis kelurusan citra landsat di Candi Umbul-Telomoyo, Provinsi Jawa Tengah. *Buletin Sumber Daya Geologi*, *6*(1), 1-10. https://doi.org/10.47599/bsdg.v6i1.92

Idroes, R., Yusuf, M., Saiful, S., Alatas, M., Subhan, S., Lala, A., Muslem, M., Suhendra, R., Idroes, G.M., Marwan, M., & Mahlia, T.M.I., 2019. Geochemistry Exploration and Geothermometry Application in the North Zone of Seulawah Agam, Aceh Besar District, Indonesia. *Energies, 12(23),* 4442. https://doi.org/10.3390/en12234442

Jin, M., Li, J., Wang, C., & Shang, R. (2015). A Practical Split-Window Algorithm for Retrieving Land Surace Temperature from Landsat-8 Data and a case Study of an Urban Area in China. *Remote Sensing, 7*, 4371–4390. https://doi.org/10.3390/rs70404371

Li, S., & Jiang, G. M. (2018). Land surface temperature retrieval from Landsat-8 data with the generalized split-window algorithm. IEEE Access, 6, 18149-18162. https://doi.org/10.1109/ACCESS.2018.2818741

Li, L., Tan, Y., Ying, S., Yu, Z., Li, Z., & Lan, H. (2014). Impact of land cover and population density on land surface temperature: case study in Wuhan, China. *Journal of applied remote sensing*, *8*(1), 084993-084993 https://doi.org/10.1117/1.JRS.8.084993

Maleki, M., Niroomand, S., Farahbakhsh, E., Modabberi, S., & Tajeddin, H.A. (2021). Hydrothermal alteration and structural mapping of the Qolqoleh-Kasnazan shear zone in Iran using remote sensing data. *Arabian Journal of Geosciences, 14.* https://doi.org/10.1007/s12517-021-07920-8

Makandar, A., & Halalli, B. (2015). Image enhancement techniques using Highpass and Lowpass filters. *International Journal of Computer Applications, 109(14)*, 12–15. https://doi.org/10.5120/19256-0999

Masoumi, F., Eslamkish, T., Honarmand, M., & Abkar, A.A. (2016). A Comparative Study of Landsat-7 and Landsat-8 Data Using Image Processing Methods for Hydrothermal Alteration Mapping. *Resource Geology, 67(1)*, 72–88. https://doi.org/10.1111/rge.12117

Mia, M. B., Fujimitsu, Y., & Nishijima, J. (2019). Exploration of hydrothermal alteration and monitoring of thermal activity using multi-source satellite images: A case study of the recently active Kirishima volcano complex on Kyushu Island, Japan. *Geothermics*, *79*, 26-45. https://doi.org/10.1016/j.geothermics.2019.01.006

Ministry of Energy and Mineral Resources - Indonesia (2022), https://www.esdm.go.id/assets/booklet/tambang-2020/Booklet-Nikel-FA.pdf (Accessed on December 2022).

Mishra, G., Govil, H., Guha, S., Monika, Tripathi, M., & Shahi, A. (2020). Comparative Evaluation of Thermal Imagery Of Landsat-8 And Aster In The Delineation Of Lithology In Jahajpur, Rajasthan, India.

Nouri, R., Jafari, M. R., Arain, M., & Feizi, F. (2012). Hydrothermal alteration zones identification based on remote sensing data in the Mahin Area, West of Qazvin Province, Iran. *Geol. Environ. Eng*, *6*(7).

Omwenga, B. M. (2020). Geothermal Well Site Suitability Selection Using Geographic Information Systems (GIS) and Remote Sensing: Case Study of the Eburru Geothermal Field. In *45th Workshop on Geothermal Reservoir Engineering* (Vol. 1, pp. 1-6).

Osinowo, O.O., Gomy, A., & Isseini, M. (2021). Mapping hydrothermal alteration mineral deposits from Landsat 8 satellite data in Pala, Mayo Kebbi Region, Southwestern Chad. *Scientific African*. https://doi.org/10.1016/j.sciaf.2020.e00687

Pour, A.B., & Hashim, M. (2012). The application of ASTER remote sensing data to porphyry copper and epithermal gold deposits. *Ore Geology Reviews, 44*. 1-9. https://doi.org/10.1016/j.oregeorev.2011.09.009

Rahmati, A.R., Moradzadeh, A., Pahlavani, P., & Rahmani, M.R. (2019). Using Index and Cumulative Overlay Analyses to Determine Geothermal Potential Targets in Damavand Region. *International Archives of the Photogrammetry, Remote Sensing and Spatial Information Sciences (ISPRS), XLII-4/W18,* 867–873. https://doi.org/10.5194/isprs-archives-XLII-4-W18-867-2019

Rani, N., Singh, T., & Mandla, V.R. (2020). Mapping hydrothermal alteration zone through aster data in Gadag Schist Belt of Western Dharwar Craton of Karnataka, India. *Environmental Earth Sciences, 79*, 526. https://doi.org/10.1007/s12665-020-09269-9

Rozenstein, O., Qin, Z., Derimian, Y., & Karnieli, A. (2014). Derivation of Land Surface Temperature for Landsat-8 TIRS Using a Split Window Algorithm. *Sensors, 14.* https://doi.org/10.3390/s140405768

Sadiya T.B., Abdulrahman, A., Sadiq, A.A., Vaatyough H.M., Ibrahim A.T., Muhammed, S.O., Ihenacho, N.M., Yusuf, M.J., Aliyu, I., Agu, N.V. (2016). Lineaments Extraction from Remote Sensing Data for Detection of Hydrothermal Alteration zones in Northern Nigeria. IOSR *Journal of Environmental Science, Toxicology and Food Technology*, *10*(4), 17-22.

Saleem, S.A., & Razak, T.A. (2014). Survey on Color Image Enhancement Techniques using Spatial Filtering. *International Journal of Computer Applications, 94(9)*, 39–45. https://doi.org/10.5120/16374-5837

Saleh, A.M. (2017). Land Surface Temperature Retrieval of Landsat-8 Data Using Split Window Algorithm-A Case Study of Mosul District. *Journal of American Science, 13(12),* 62–75. https://doi.org/10.7537/marsjas131217.08

Sekertekin, A., & Bonafoni, S. (2020). Land Surface Temperature Retrieval from Landsat 5, 7, and 8 over Rural Areas: Assessment of Different Retrieval Algorithms and Emissivity Models and Toolbox Implementation. *Remote Sensing, 12*. https://doi.org/10.3390/rs12020294

Şener, E., & Şener, Ş. (2021). Exploration of geothermal potential using integrated fuzzy logic and analytical hierarchy process (AHP) in Ağrı, Eastern Turkey. *Turkish Journal of Earth Sciences, 30*, 1134–1150. https://doi.org/10.3906/yer-2105-18

Sheikhrahimi, A., Pour, A.B., Pradhan, B., & Zoheir, B. (2019). Mapping hydrothermal alteration zones and lineaments associated with orogenic gold mineralization using ASTER data: A case study from the Sanandaj-Sirjan Zone, Iran. *Advances in Space Research*. https://doi.org/10.1016/j.asr.2019.01.035

Shi, D., & Yang, X. (2015). Support vector machines for land cover mapping from remote sensor imagery. *Monitoring and Modeling of Global Changes: A Geomatics Perspective*, 265-279. https://doi.org/10.1007/978-94-017-9813-6_13

Southworth, J. (2004). An assessment of Landsat TM band 6 thermal data for analysing land cover in tropical dry forest regions. *International Journal of Remote Sensing, 25(4)*, 689-706. https://doi.org/10.1080/0143116031000139917

Sugianto, S., Rusdi, M., Budi, M., Farhan, A., & Akhyar, A. (2023). Agricultural Droughts Monitoring of Aceh Besar Regency Rice Production Center, Aceh, Indonesia–Application Vegetation Conditions Index using Sentinel-2 Image Data. *Journal of Ecological Engineering*, *24*(1).

Sutanto. (1987). Penginderaan Jauh *Jilid 2. Yogyakarta: Gadjah Mada University Press*. (in Indonesia) https://onesearch.id/Record/IOS2862.UNMAL000000000000323

Tan, K., Liao, Z., Du, P., & Wu, L. (2016). Land surface temperature retrieval from Landsat 8 data and validation with geosensor network. Front. *Earth Sci*. https://doi.org/10.1007/s11707-016-0570-7

Twumasi, Y. A., Merem, E. C., Namwamba, J. B., Mwakimi, O. S., Ayala-Silva, T., Frimpong, D. B., ... & Mosby, H. J. (2021). Estimation of land surface temperature from Landsat-8 OLI thermal infrared satellite data. A comparative analysis of two cities in Ghana. *Advances in Remote Sensing*, *10*(4), 131-149. https://doi.org/10.4236/ars.2021.104009

Ulivieri, C. M. M. A., Castronuovo, M. M., Francioni, R., & Cardillo, A. (1994). A split window algorithm for estimating land surface temperature from satellites. *Advances in Space Research*, *14*(3), 59-65. https://doi.org/10.1016/0273-1177(94)90193-7

Waldhoff, G., Bubenzer, O., Bolten, A., Koppe, W., Bareth, G. (2008). Spectral Analysis of ASTER, HYPERION, and QUICKBIRD Data for Geomorphological and Geological Research in Egypt (Dakhla Oasis, Western Desert). *The International Archives of the Photogrammetry, Remote Sensing and Spatial Information Sciences*. XXXVII. XXXVIII. Spat. Inf. Sci, 37, 1201-1206.

Zhang, S., Duan, S., Li, Z., Huang, C., Wu, H., Han, X., Leng, P., & Gao, M. (2019). Improvement of Split-Window Algorithm for Land Surface Temperature Retrieval from Sentinel-3A SLSTR Data Over Barren Surface Using ASTER GED Product. *Remote Sensing, 11*. https://doi.org/10.3390/rs11243025

Zhao, W., Dong, Q., Chen, Z., Feng, T., Wang, D., Jiang, L., ... & Chen, J. (2021). Weighted information models for the quantitative prediction and evaluation of the geothermal anomaly area in the plateau: a case study of the Sichuan–Tibet Railway. *Remote Sensing*, *13*(9), 1606. https://doi.org/10.3390/rs13091606